

# A Comparative Study on 1.5T - 3T MRI Conversion through Deep Neural Network Models

Binhua Liao<sup>\*†</sup>, Yani Chen<sup>\*</sup>, Zhewei Wang<sup>\*</sup>, Charles D. Smith<sup>‡</sup>, Jundong Liu<sup>\*</sup>

<sup>\*</sup>School of Electrical Engineering and Computer Science, Ohio University, USA

<sup>†</sup>College of Mathematics and Statistics, Huazhong Normal University, PR China

<sup>‡</sup>Department of Neurology, University of Kentucky, USA

**Abstract**—In this paper, we explore the capabilities of a number of deep neural network models in generating whole-brain 3T-like MR images from clinical 1.5T MRIs. The models include a fully convolutional network (FCN) method and three state-of-the-art super-resolution solutions, ESPCN [26], SRGAN [17] and PRSR [7]. The FCN solution, U-Convert-Net, carries out mapping of 1.5T-to-3T slices through a U-Net-like architecture, with 3D neighborhood information integrated through a multi-view ensemble. The pros and cons of the models, as well as the associated evaluation metrics, are measured with experiments and discussed in depth. To the best of our knowledge, this study is the first work to evaluate multiple deep learning solutions for whole-brain MRI conversion, as well as the first attempt to utilize FCN/U-Net-like structure for this purpose.

**Index Terms**—FCN, MRI, modality conversion, U-Net, U-Convert-Net, GAN, SRGAN

## I. INTRODUCTION

Magnetic resonance imaging (MRI) is widely used in neuroimaging and the popularity is due to its non-invasive nature, high soft tissue contrast, as well as the availability of safe intracellular contrast agents. Currently 1.5 tesla (T) short-bore MRI is the standard technology for clinical use. However, 3T (and even 7T) MRI scanners are becoming increasingly more desirable, as they can provide extremely clear and vivid images. Comparing with 1.5T, 3T MR images have higher signal-to-noise ratios (SNR) and higher contrast-to-noise ratios (CNR) between gray and white matter. The latter make 3T MRI a better choice for brain tissue segmentation, as well as a generally preferred modality in neuroimaging studies.

While the availability of 3T MRI has increased significantly over the past decade, the majority of clinical scanners across the US are still 1.5T systems. Converting 1.5T images into 3T-like images, if with great fidelity, would help physicians make better informed diagnosis and treatment decisions. In addition, historical 1.5T MR images in various ongoing longitudinal studies can also be brought into a better use. One of such examples is the Alzheimer’s Disease Neuroimaging Initiative (ADNI) project – 1.5T was the major MRI modality in ADNI 1, the first stage of the project, but the acquisition switched to 3T alone in later stages (ADNI GO, 2 and 3). Converting 1.5T images into 3T-like counterparts may allow the datasets generated in such studies to be delivered in a more uniform form.

Establishing a nonlinear spatially-varying intensity mapping between two images is a challenging task. The efforts to tackle this problem can trace back to at least the *Image Analogies* model [12], which relies on a nonparametric texture model [9] to learn the mapping on a single pair of input-output images. The emerge of the powerful deep learning paradigm in recent years makes the task more viable. *Generative adversarial networks* (GAN) [15], [17], [34], [37], [41] and pixel-RNN/CNN [7] are among the models that have been applied for modality conversion, producing impressive results.

The original GAN model by Goodfellow *et al.* [11] was designed to generate images that are similar to the training samples. Several later solutions, including DualGAN [37], CycleGAN [41] and DiscoGAN [16], take the similar idea to train image-to-image translation with unpaired natural images. The CycleGAN model has been adopted to synthesize CT images from MRIs [34]. While flexible and with broad applicability, this group of solutions rely on the distribution of real samples instead of paired inputs/outputs, even if the latter are available. Consequently, the results from this group can be rather unstable and far from uniformly positive [41]. Some GANs, including pix2pix [15] and PAN [31], take paired training samples to trade flexibility for stability.

With paired input/output samples, MR modality conversion could be implemented as a special case of super-resolution, where one or multiple low-resolution images are combined to generate images with higher spatial resolution. Traditional super-resolution solutions include reconstruction-based methods [25], [27], [30], [35], and example-based methods [3], [10], [14], [20], [24], [36], [39]. Under the deep learning framework, numerous new super-resolution solutions have recently been developed, in both the computer vision [7], [26] and medical image computing [2], [1], [8], [18], [28], [40] communities. SRGAN [17], a model designed to recover the finer texture details even with large upscaling factors, is commonly regarded as one of the state-of-the-art solutions.

Fully convolutional networks (FCN) proposed by Long *et al.* [19] was primarily designed for image segmentation, which can also be regarded as a special type of modality mapping – from gray-valued intensities to binary-valued labels. U-Net [23] and its variants [4], [5], [29], [32], [33] follow the similar idea of FCN and rely on skip connections to concatenate features from the contracting (convolution) and expanding

## SRGAN for image translation

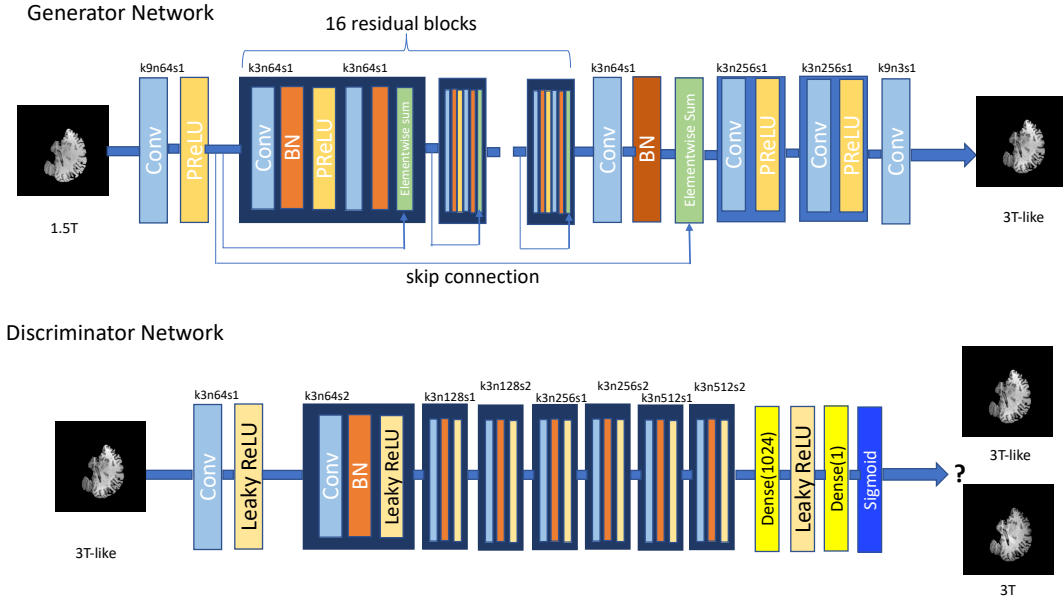


Fig. 1: The overall architecture of SRGAN for MRI conversion: generator and discriminator with corresponding kernel size (k), number of feature maps (n) and stride (s) indicated for each convolutional layer.

(deconvolution) paths. In theory, an FCN with a proper setup can potentially describe any intensity mapping between two modalities. However, such capacity of FCN has yet been explored for general-purpose modality conversion. It should be noted that, Nie *et al.* [21] use a convolutional network for MR to CT conversion, but their network structure is not FCN/U-Net equivalent, as no pooling, skip connections, contracting and expanding components are utilized.

In this paper, we explore the capability of a number of super-resolution (SR) and segmentation models in handling modality conversion. More specifically, we adopt SR models including ESPCN [26], SRGAN and PRSR [7], and modify Chen’s segmentation model [5], to convert 1.5T whole-brain MR images into 3T. Experiments are conducted with ADNI data. To the best of our knowledge, this study is the first work to compare and evaluate multiple deep learning solutions, based on various performance metrics, for whole-brain MRI conversion.

## II. METHOD

The MR conversion models to be analyzed in this study are modified from SR and segmentation solutions, respectively. In this section, we introduce them in detail.

### A. Modified from Super-Resolution Solutions

**SRGAN** is designed to generate  $4\times$  upscaled photo-realistic natural images with highly perceptual quality. Focused on recovering finer texture details in up-scaled images, SRGAN adopts a perceptual loss function that consists of an adversarial

loss and a content loss. As a super-resolution solution, SRGAN produces outputs that have different sizes from inputs. To suit for our MRI conversion task, we remove one upsampling layer to make the input/output of equal size.

As shown in Fig. 1, the modified SRGAN for MR conversion model consists of two major components: generator and discriminator. The generator part is a deep residual network (ResNet) with skip-connections, generating 3T-like images from 1.5T inputs. The goal of the generator is to be able to produce 3T images so realistic that it would be able to fool the discriminator. The discriminator, on the other hand, is configured as a classification CNN and its goal is to be trained as sharp as possible to distinguish fake 3T from real 3T images. With this setup, the generator can eventually learn to create outputs that are highly similar to real 3T images.

**ESPCN** uses two convolutional layers to extract feature maps from low resolution image and then applies a sub-pixel convolution layer to transform these feature maps back to an enlarged super resolution image. The sub-pixel layer is designed to be very efficient, which reduces the computational complexity of the model and enables the system to achieve real-time super-resolution of 1080p videos on a single K2 GPU.

**PRSR** is a super resolution model build upon ResNet and PixelCNNs (a probabilistic generative model) that is capable of enlarging small input image to a wide range of plausible high-resolution images with large amplification factors. Experiments show that the transformed images obtain high rate of perceptual evaluation by humans.

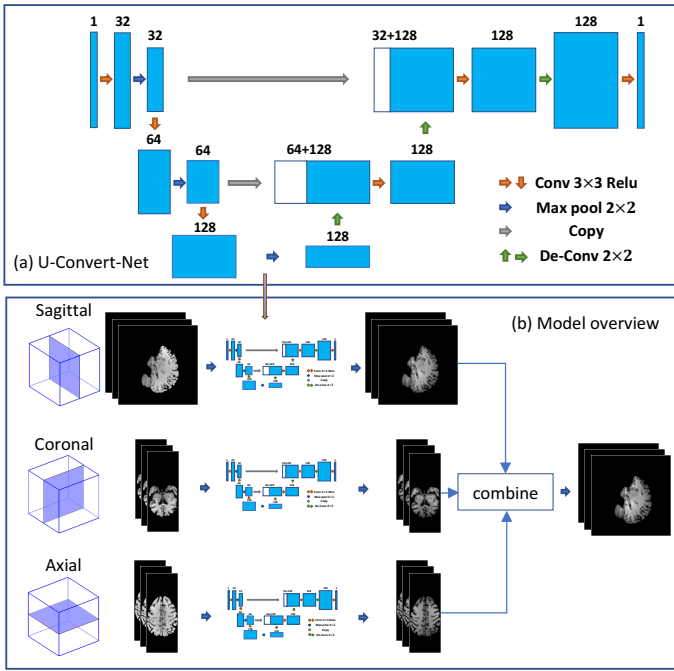


Fig. 2: The overall architecture of Multi-view U-Convert-Net: (a) U-Convert-Net and (b) Model overview.

### B. Modified from FCN-based Segmentation Solution

As shown in Fig. 2, the segmentation-based model consists of two major components. First, U-Convert-Net, a U-Net-like network, is trained to convert two-dimensional (2D) slices extracted from 1.5T MR volumes into slices of 3T MR images. Second, the converted 3T slices from three different views are fused together to generate the final 3T MR volumes with enhanced structural details and intensity contrasts.

The main architecture of U-Convert-Net is modified from U-Net [23]. Similar to U-Net, our U-Convert-Net (shown in Fig. 2(a)) is also comprised of encoding and decoding paths. 1.5T MR slices are inputs and go through several “convolution + pooling” layers to be encoded into high-level latent features. These features will then be sent through several “deconvolution/upsampling” layers to reconstruct the target 3T MR images. Structural information lost during the pooling procedure would be added back through “bridges”: latent features in the encoded path are concatenated with the corresponding feature maps from the decoding path.

U-Convert-Net is different from U-Net in several aspects. The first major alternation is to the loss function. U-Net uses cross-entropy as their loss, which is a reasonable choice to seek for intensity-to-label mappings. For intensity-to-intensity translation, mean-square-error (MSE) would be more appropriate, as any deviation from the target 3T image should be penalized.

The second set of modifications are made in order to reduce the training time and make the structure reusable for different views, whose input image dimensions may be different. We use padded convolution to maintain the same spatial dimension

of the data flow throughout the convolutional layers. This is in contrast with U-Net, where the images are altered at input to accommodate dimension decrement along convolutions. We only keep one convolutional layer prior to each pooling layer to reduce the number of parameters of the network. The size of the filters is kept as  $3 \times 3$ . Third, to ease the training procedure, explicit data augmentation as in U-Net, which would increase training time, is replaced with dropout operations on several deconvolution layers to prevent overfitting. Additionally, in the last convolution layer, the transformed 2D images are generated by applying only one  $3 \times 3$  filter.

With the 2D images generated from individual slices, an overall 3D image can be obtained by stacking these 2D image slices back together. A limitation of such slice-based 3D transformation is that the contextual information between slices is overlooked and not taken into account to generate the overall conversion. Our strategy to tackle this issue is to combine the conversion results from three orthogonal views – sagittal, coronal and axial. While not directly extracting 3D information from sub-volumes, slices from these orthogonal views do contain complementary information, enough to depict the 3D neighborhood surrounding each voxel.

FCN/U-Net segmentation can also be carried out with 3D convolutions [6], but we believe our “2D U-Convert-Net+ multi view” have several practical advantages, especially for whole-brain neuroimage analyses.

### C. Loss Functions and Evaluation Metrics

As mentioned in last section, the objective to be optimized in our U-Convert-Net is the mean squared error (MSE) between the generated 3T images and ground truth. This is also a very common setup in SR algorithms, as minimizing MSE also maximizes the peak signal-to-noise ratio (PSNR), which is a well-accepted measure used to evaluate and compare SR algorithms [38]. Structural similarity index (SSIM) is another widely used evaluation metric in SR studies. PSNR is good at showing absolute errors, while SSIM focuses more on structural resemblance which carry important information on human’s visual scene.

However, minimizing MSE tends to produce blurry results [22], [38]. This is because the minimum of MSE would be the average of all possible samples, which leads to blurring. Identifying loss functions that can force FCN-like models to produce sharp, realistic images, is still an open problem and may have to be application-dependent.

GAN models are designed, to certain extent, to tackle this issue. GANs, including SRGAN, learn a loss that trains the discriminator to be intelligent at identifying if the output image is real or fake, while simultaneously train the generator to minimize this loss. Blurry images will be rejected as they do not look real. The perceptual loss adopted in SRGAN consists of an adversarial loss and a content loss. Minimizing the content loss would increase the similarity, perception-wise instead of pixel-wise, between the generated images and the target.

The enhanced conversion quality obtained in SRGAN, however, is not reflected in the evaluations with traditional metrics – SGRAN is outperformed by its MSE-based version measured with PSNR. The authors of SRGAN had to resort to a subjective metric called *mean opinion score* (MOS) to demonstrate the improvements. In MOS, human raters are called in to assign integral scores to assess the obtained results.

We are well aware of the above issues, and take them into account in our experiment designs for MR conversion, as well as the analysis of the results.

### III. EXPERIMENTS

#### A. Data, Preprocessing, and Evaluation Metrics

The data used in this work were obtained from the ADNI database [13]. Started in 2004, ADNI is currently in the stage of ADNI 3, after the completion of ADNI 1, GO and 2. The participants enrolled in late stages (GO/2/3) were scanned using the 3T MRI scanning protocols. In ADNI 1, however, subjects were scanned using either a 1.5T scanner, or both 1.5T and 3T scanners. MR images acquired in the latter generates a considerable number of matched 1.5T/3T pairs (in the sense of same person in the same visit). We searched the ADNI database for these cases, and downloaded all the 1.5T/3T pairs acquired in the same visits (one pair each visit). To simplify our network design, we chose the largest subset of the images that have the same resolutions/sizes, which results in 157 distinct pairs of 1.5T/3T images, from 47 different subjects.

A series of pre-processing steps were then applied. Firstly, each MRI pair was spatially aligned using SPM12. The skulls were removed, and the image size was uniformly reduced to  $(256 \times 256 \times 100)$  after removing a number of empty slices. As the 3T images in ADNI GO/2/3 were all acquired along the sagittal view, each 1.5T MR image was aligned with their 3T counterpart, and resampled into 2D slices along the same axis. These 157 pairs of images are the training samples in this study. In our experiments, we randomly chose 90% of subjects (totally 141) for training, and the remaining one tenth (16) for testing.

As mentioned in the previous section, the similarity between the generated 3T images and ground truth are measured using SSIM and PSNR. We also qualitatively look into the image contrast at various areas, including the boundaries between gray matter and white matter.

#### B. Results

All the experiments were conducted on an NVidia GTX 1080 GPU (2560 CUDA Cores, 8 GB GDDR5X Memory) using TensorFlow package. We design a number of experiments to evaluate our model, as well as the competing solutions. The tests are on running-time and conversion accuracy, respectively.

**Experimental design** Through early experiments, we observed that the four models had rather different performance in terms of running time. PRSR was very slow, and would take a prohibitively long time to process the original  $256 \times 256$  sized images. Therefore, we design the first experiment to

specifically evaluate the time performance of the models. In order to ensure PRSR to run through, we reduce the image size to  $96 \times 96$  in this experiment. The results will be reported shortly. The other three models can take the  $256 \times 256$  sized images, though still with rather different GPU times. The second experiment is designed to evaluate the accuracies of modality conversion of the models. Training and testing are conducted on the original image pairs, with PRSR being excluded for comparison. The third experiment is to evaluate the effectiveness of multi-view ensemble, when integrated on top of U-Convert-Net.

The training details of the first two experiments, including image sizes, learning rates, training time and testing time, are listed in Table 1. In experiment 3, the same settings have been used for the U-Convert-Nets on coronal and axial views. All the experiments were run over 40 epochs.

TABLE I: Training details of the experiments: image sizes, learning rates (lr), batch sizes, training time (seconds per epoch) and testing time (seconds per image).

image size	...	PRSR	SRGAN	ESPCN	U-Convert-Net
exp1 96×96	lr	0.004	0.001	0.002	0.001
	batch	4	4	4	4
	training	1666	1998	92	203
	testing	1921	0.005	0.005	0.005
exp2 256×256	lr	–	0.001	0.001	0.001
	batch	–	1	4	4
	training	–	8979	118	313
	testing	–	0.005	0.005	0.005

**Running time comparison** The results are shown in Table I. For the tests on  $96 \times 96$  sized images, ESPCN is the fastest, followed by U-Convert-Net, PRSR and SRGAN. PRSR takes much longer time in testing, as pixels need to be generated one-by-one in a serial order. In the tests for the full-sized images (experiment 2), ESPCN is still the fastest. This is due to the efficient design in ESPCN that specifically shortcuts the deconvolution operations. Our U-Convert-Net is slower than ESPCN, but is 28 times faster than SRGAN. This can be partially explained by the fact that SRGAN employs ResNet, with much more layers than U-Convert-Net.

TABLE II: System performance measured with SSIM and PSNR.

.....	ESPCN	SRGAN	U-Convert-Net	U-Convert-Net+3Vs
SSIM	0.85	0.94	0.93	0.94
PSNR	21.8	25.1	26.5	28.4

**Conversion Accuracy by Traditional Metrics** The quantitative evaluations of the solutions, measured with SSIM and PSNR, is shown in Table II. All the measurements are conducted on the 2D slices extracted from the sagittal view. It can be observed that U-Convert-Net achieves better performance than ESPCN and SRGAN in terms of PSNR. For SSIM, U-Convert-Net is better than ESPCN and is comparable with SRGAN but with a much shorter training time. The effectiveness of multi-view ensemble is validated in experiment 3: in addition to the original sagittal-view slices/results, we conduct the network constructions and trainings for the slices

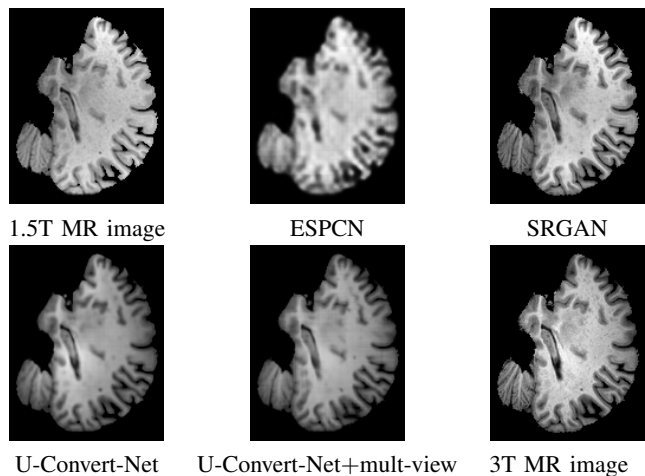


Fig. 3: Source (1.5T), target (3T) and the generated 3T MR images using different models. Figures are best viewed on screen.

along coronal and axial views. The 3T conversion volumes of the three views are averaged to produce the final output of our multi-view U-Convert-Net. As shown in the last column of Table II, both SSIM and PSNR are improved through the view ensemble.

**Actual Contrast Enhancements** A major advantage of 3T MRIs over 1.5T is the enhanced contrasts along the boundaries of gray and white matter. To get a qualitative comparison, we also look into the 3T images produced by the models. Fig. 3 shows the zoom-in version of a typical slice. Obviously ESPCN’s high speed comes with a cost – its 3T result is over smoothed with missing details. Results from SRGAN, U-Convert-Net and its multi-view version are all consistent with the ground-truth 3T image.

The comparison between multi-view U-Convert-Net and SRGAN reveals the deficiencies of the traditional metrics. While the former has a “superior” performance measured by PSNR and SSIM, SRGAN obviously generates slices that have higher contrasts between gray and white matter, as shown in Fig. 3. This observation is consistent with the experiments conducted in SRGAN paper [17], where the proposed method (SRGAN) gets lower PSNR and SSIM measures than its MSE version, but performs better in the subjective metric MOS, judged by human raters.

All in all, our observations can be summarized as: 1) SRGAN can produce higher contrasts MR images with the help of its discriminator; 2) the multi-view U-Convert-Net framework produces results with higher PSNR and SSIM measures; 3) multi-view U-Convert-Net framework can be trained much faster than SRGAN.

#### IV. CONCLUSIONS

In this work, we study four solutions for MRI modality conversion. The models are compared and evaluated with various metrics. The FCN-based Multi-view U-Convert-Net is fast to train and it achieves the better performance in

1.5 to 3T MRI mapping, measured with SSIM and PSNR. SRGAN, on the other hand, produces more realistic 3T-like images with enhanced contrasts. The take-home messages could be: 1) GAN models have inherent mechanism for image conversions, including that between MRIs; 2) FCNs equipped with other loss functions, including perception-based losses, are also worth explorations for faster solutions.

#### REFERENCES

- [1] K. Bahrami *et al.*, “Convolutional neural network for reconstruction of 7t-like images from 3t mri using appearance and anatomical features,” in *DLMIA. Vol. 10008 of Lect Notes Comput Sci.*, 2016, pp. 39–47.
- [2] —, “Reconstruction of 7t-like images from 3t mri,” *IEEE transactions on medical imaging*, vol. 35, no. 9, pp. 2085–2097, 2016.
- [3] N. Burgos *et al.*, “Attenuation correction synthesis for hybrid pet-mr scanners: application to brain studies,” *IEEE transactions on medical imaging*, vol. 33, no. 12, pp. 2332–2341, 2014.
- [4] Y. Chen, B. Shi, Z. Wang, T. Sun, C. D. Smith, and J. Liu, “Accurate and consistent hippocampus segmentation through convolutional lstm and view ensemble,” in *International workshop on machine learning in medical imaging*. Springer, 2017, pp. 88–96.
- [5] Y. Chen, B. Shi, Z. Wang, P. Zhang, C. D. Smith, and J. Liu, “Hippocampus segmentation through multi-view ensemble convnets,” in *2017 IEEE 14th international symposium on biomedical imaging (ISBI 2017)*. IEEE, 2017, pp. 192–196.
- [6] Ö. Çiçek *et al.*, “3d u-net: learning dense volumetric segmentation from sparse annotation,” in *International Conference on Medical Computing and Computer-Assisted Intervention*. Springer, 2016, pp. 424–432.
- [7] R. Dahl *et al.*, “Pixel recursive super resolution,” *arXiv preprint arXiv:1702.00783*, 2017.
- [8] S. C. Deoni *et al.*, “Simultaneous high-resolution t2-weighted imaging and quantitative t2 mapping at low magnetic field strengths using a multiple te and multi-orientation acquisition approach,” *Magnetic Resonance in Medicine*, 2022.
- [9] A. A. Efros and T. K. Leung, “Texture synthesis by non-parametric sampling,” in *Computer Vision, 1999. The Proceedings of the Seventh IEEE International Conference on*, vol. 2. IEEE, 1999, pp. 1033–1038.
- [10] X. Gao *et al.*, “Image super-resolution with sparse neighbor embedding,” *IEEE Transactions on Image Processing*, vol. 21, no. 7, pp. 3194–3205, 2012.
- [11] I. Goodfellow, J. Pouget-Abadie, M. Mirza, B. Xu, D. Warde-Farley, S. Ozair, A. Courville, and Y. Bengio, “Generative adversarial nets,” in *Advances in neural information processing systems*, 2014, pp. 2672–2680.
- [12] A. Hertzmann, C. E. Jacobs, N. Oliver, B. Curless, and D. H. Salesin, “Image analogies,” in *Proceedings of the 28th annual conference on Computer graphics and interactive techniques*. ACM, 2001, pp. 327–340.
- [13] A. D. N. I. A. <http://www.loni.usc.edu/ADNI>.
- [14] T. Huynh *et al.*, “Estimating ct image from mri data using structured random forest and auto-context model,” *IEEE transactions on medical imaging*, vol. 35, no. 1, pp. 174–183, 2016.
- [15] P. Isola, J.-Y. Zhu, T. Zhou, and A. A. Efros, “Image-to-image translation with conditional adversarial networks,” *arXiv preprint arXiv:1611.07004*, 2016.
- [16] T. Kim, M. Cha, H. Kim, J. K. Lee, and J. Kim, “Learning to discover cross-domain relations with generative adversarial networks,” *CoRR*, vol. abs/1703.05192, 2017. [Online]. Available: <http://arxiv.org/abs/1703.05192>
- [17] C. Ledig *et al.*, “Photo-realistic single image super-resolution using a generative adversarial network,” *arXiv preprint arXiv:1609.04802*, 2017.
- [18] C. Liu *et al.*, “Fusing multi-scale information in convolution network for mr image super-resolution reconstruction,” *Biomedical engineering online*, vol. 17, no. 1, pp. 1–23, 2018.
- [19] J. Long *et al.*, “Fully convolutional networks for semantic segmentation,” in *Proceedings of the IEEE Conference on CVPR*, 2015, pp. 3431–3440.
- [20] J. V. Manjón *et al.*, “Mri superresolution using self-similarity and image priors,” *Journal of Biomedical Imaging*, vol. 2010, p. 17, 2010.
- [21] D. Nie *et al.*, “Estimating ct image from mri data using 3d fully convolutional networks,” in *DLMIA 2016, Held in Conjunction with MICCAI 2016*, 2016, pp. 1529–1537.

- [22] D. Pathak, P. Krahenbuhl, J. Donahue, T. Darrell, and A. A. Efros, "Context encoders: Feature learning by inpainting," in *Proceedings of the IEEE Conference on Computer Vision and Pattern Recognition*, 2016, pp. 2536–2544.
- [23] O. Ronneberger *et al.*, "U-net: Convolutional networks for biomedical image segmentation," in *International Conference on MICCAI*. Springer, 2015, pp. 234–241.
- [24] S. Roy *et al.*, "Magnetic resonance image example-based contrast synthesis," *IEEE transactions on medical imaging*, vol. 32, no. 12, pp. 2348–2363, 2013.
- [25] F. Shi *et al.*, "Lrtv: Mr image super-resolution with low-rank and total variation regularizations," *IEEE transactions on medical imaging*, vol. 34, no. 12, pp. 2459–2466, 2015.
- [26] W. Shi *et al.*, "Real-time single image and video super-resolution using an efficient sub-pixel convolutional neural network," *arXiv preprint arXiv:1609.05158*, 2016.
- [27] R. Z. Shilling *et al.*, "A super-resolution framework for 3-d high-resolution and high-contrast imaging using 2-d multislice mri," *IEEE transactions on medical imaging*, vol. 28, no. 5, pp. 633–644, 2009.
- [28] K. Srinivasan *et al.*, "Realizing the effective detection of tumor in magnetic resonance imaging using cluster-sparse assisted super-resolution," *The Open Biomedical Engineering Journal*, vol. 15, no. 1, 2021.
- [29] T. Sun, Z. Wang, C. Smith, and J. Liu, "Tracecaps: A capsule-based neural network for semantic segmentation," *arXiv preprint arXiv:1901.02920*, 2019.
- [30] E. Van Reeth *et al.*, "Super-resolution in magnetic resonance imaging: A review," *Concepts in Magnetic Resonance Part A*, vol. 40, no. 6, pp. 306–325, 2012.
- [31] C. Wang, C. Xu, C. Wang, and D. Tao, "Perceptual adversarial networks for image-to-image transformation," *CoRR*, vol. abs/1706.09138, 2017. [Online]. Available: <http://arxiv.org/abs/1706.09138>
- [32] Z. Wang, W. Cai, C. D. Smith, N. Kantake, T. J. Rosol, and J. Liu, "Residual pyramid fcn for robust follicle segmentation," in *2019 IEEE 16th International Symposium on Biomedical Imaging (ISBI 2019)*. IEEE, 2019, pp. 463–467.
- [33] Z. Wang, C. D. Smith, and J. Liu, "Ensemble of multi-sized fcns to improve white matter lesion segmentation," in *International Workshop on Machine Learning in Medical Imaging*. Springer, 2018, pp. 223–232.
- [34] J. Wolterink *et al.*, "Deep mr to ct synthesis using unpaired data," *arXiv preprint arXiv:1708.01155*, 2017.
- [35] J. Woo *et al.*, "Super-resolution reconstruction for tongue mr images," in *Proceedings of SPIE*, vol. 8314. NIH Public Access, 2012.
- [36] J. Yang *et al.*, "Coupled dictionary training for image super-resolution," *IEEE transactions on image processing*, vol. 21, no. 8, pp. 3467–3478, 2012.
- [37] Z. Yi *et al.*, "Dualgan: Unsupervised dual learning for image-to-image translation," *arXiv preprint arXiv:1704.02510*, 2017.
- [38] R. Zhang, P. Isola, and A. A. Efros, "Colorful image colorization," in *European Conference on Computer Vision*. Springer, 2016, pp. 649–666.
- [39] Y. Zhang *et al.*, "Hierarchical patch-based sparse representation? a new approach for resolution enhancement of 4d-ct lung data," *IEEE transactions on medical imaging*, vol. 31, no. 11, pp. 1993–2005, 2012.
- [40] X. Zhao *et al.*, "Accurate mr image super-resolution via lightweight lateral inhibition network," *Computer Vision and Image Understanding*, vol. 201, p. 103075, 2020.
- [41] J. Zhu *et al.*, "Unpaired image-to-image translation using cycle-consistent adversarial networks," *arXiv preprint arXiv:1704.02510*, 2017.